Assessment of Lymph Node Metastases by Contrast-Enhanced MR Imaging in a Head and Neck Cancer Model

Ki Chang Lee, DVM, PhD[1]
Woo Kyung Moon, MD[2]
Jin Wook Chung, MD[2]
Seung Hong Choi, MD[2]
Nariya Cho, MD[2]
Joo Hee Cha, MD[2]
Eun Hye Lee, MD[2]
Sun Mi Kim, MD[2]
Hoe Suk Kim, PhD[3]
Moon Hee Han, MD[2]
Kee-Hyun Chang, MD[2]

Index terms:
Lymphatic system, diseases
Magnetic resonance (MR), contrast media
Head and neck neoplasms, MR
Experimental study

Korean J Radiol 2007;8:9-14
Received January 21, 2006; accepted after revision April 3, 2006.

[1]Department of Veterinary Radiology, Chonbuk National University College of Veterinary Medicine, Jeonju City 560-700, Korea; [2]Department of Radiology, Seoul National University College of Medicine and The Institute of Radiation Medicine, Seoul National University Medical Research Center, Seoul 110-744, Korea; [3]Institute of Life Science and Biotechnology, Yonsei University

Supported by a grant from the Seoul R & BD the Program and National R & D Program for Cancer Control, Ministry of Health & Welfare, Republic of Korea (0420080-1).

Address reprint requests to:
Woo Kyung Moon, MD, Department of Radiology, Seoul National University Hospital, 28, Yongon-dong, Chongno-gu, Seoul 110-744, Korea.
Tel. (822) 2072-3928
Fax. (822) 743-6385
e-mail: moonwk@radcom.snu.ac.kr

Objective: We wanted to investigate the accuracy of contrast-enhanced MR imaging for the detection of lymph node metastases in a head and neck cancer rabbit model.

Materials and Methods: The metastatic lymph node model we used was created by inoculating VX2 tumors into the auricles of six New Zealand White rabbits. T1-weighted MR images were obtained before and after injecting gadopentetate dimeglumine at three weeks after tumor cell inoculation. The sizes, signal intensity ratios (i.e., the postcontrast signal intensities of the affected nodes relative to the adjacent muscle) and the enhancement patterns of 36 regional lymph nodes (parotid and caudal mandibular nodes) were evaluated on MR images and then compared with the histopathologic findings.

Results: No statistical difference was found between the sizes of 12 metastatic (10.5 ± 3.2 mm) and 24 hyperplastic (8.0 ± 3.6 mm) lymph nodes ($p > 0.05$). On the contrast-enhanced T1-weighted MR images, nine metastatic and four hyperplastic lymph nodes had peripheral high and central low signal intensity, whereas three metastatic and 20 hyperplastic lymph nodes had homogeneous high signal intensity. Using a signal intensity ratio less than one as a diagnostic criterion for a metastatic lymph node, the sensitivity, specificity and positive and negative predictive values of the enhanced MR images were 75% (9/12), 83% (20/24), 69% (9/13) and 87% (20/23), respectively, with areas under receiver-operating-characteristic curve values of 0.81.

Conclusion: This experimental study confirms that metastatic and hyperplastic lymph nodes can be differentiated using MR images on the basis of the contrast uptake patterns, but that they cannot be differentiated using any particular size criteria.

The detection of metastasis to lymph nodes is critical for the tumor staging and preoperative planning in patients with head and neck cancer (1–3). Contrast material enhanced computed tomography (CT) and conventional magnetic resonance (MR) imaging are limited in terms of their abilities to detect metastatic disease in the normally sized lymph nodes because the diagnostic criteria that are used are based on lymph node size and shape (4–6). However, the use of contrast agent can improve both the sensitivity and specificity of nodal evaluation by MR imaging because the identification of necrosis is a reliable sign of a metastatic node (7–11).

The development of an adequate animal model would be quite useful to compare the accuracies of different imaging modalities or different contrast agents with respect to nodal evaluation. The VX2 tumor inoculated into the auricles shows rapid growth,

and lymph node metastases are almost always observed in the parotid gland within 21 days of subcutaneous implantation (12). This metastatic model has been used to study the sentinel node concept and to evaluate the effects of antitumor agent in the context of human head and neck squamous cell carcinoma (12, 13). But to the best of our knowledge, this head and neck carcinoma model has not been used for contrast-enhanced MR imaging.

The purpose of this study was to investigate the accuracy of contrast-enhanced MR imaging for the detection of lymph node metastases in a head and neck cancer rabbit model.

MATERIALS AND METHODS

Animals and the Experimental Design

All the studies were conducted with the approval of the animal care committee at Seoul National University Hospital. The experiments were performed using six New Zealand White rabbits (Central Biological Laboratory, Seoul, Korea) weighing 2.5−3.0 kg each. The animals were allowed food and water ad libitum between the various procedures. They were anesthetized by an intramuscular injection of 50 mg/kg of ketamine hydrochloride (Ketalar®, Yuhan Yanghang, Seoul, Korea) and 20 mg/kg xylazine hydrochloride (Rompun® Bayer Korea, Seoul, Korea).

To induce head and neck cancer, 0.5 ml of a cell suspension of VX2 carcinoma was inoculated subcutaneously into the cranial section of the lower third of both auricles. The experimental auricular VX2 rabbit carcinoma was prepared in a manner described previously (12). The MR imaging was performed approximately three weeks after VX2 inoculation. Solid auricular masses were palpable in all animals.

MR Imaging

The anesthetic regimen used for tumor implantation was also used for MR imaging. The ear vein of a rabbit was cannulated with a 22-gauge infusion set that was connected to a 1 mL syringe loaded with contrast agent. All the animals were imaged in the prone position. All examinations were performed using a 1.5-T superconducting magnet (Signa Horizon, GE Medical Systems, Milwaukee, WI) and with employing a standard transmit-receive quadrature head coil. After obtaining the routine localization images, the T1-weighted spin-echo (SE) sequence was performed in the coronal plane with using the following parameters: a TR of 400 ms, a TE of 12 ms and two excitations. The slice thickness used was 2 mm without a gap, the matrix number was 256 ×160 and the field of view (FOV) was 16 cm. The T2-weighted fast SE sequence (TR/TE: 3500/84 ms, 2 excitations) was also obtained. The coronal three-dimensional fast spoiled gradient-recalled echo (3D-SPGR) T1-weighted images (TR/TE, 19.7/1.8 ms; FOV, 20 ×20 cm) were obtained before and 2 minutes after 0.1 mmol/kg of body weight gadopentetate dimeglumine (Magnevist® Schering, Germany) had been administered by manual injection via an ear vein.

Image Analysis

All MR images were assessed with an emphasis placed on the parotid and caudal mandibular lymph nodes. The images were retrospectively evaluated by consensus between two experienced radiologists (who unaware of the study details) for the lymph node size, the signal intensity ratios and the enhancement pattern. No attention was paid to the stage of the auricle carcinoma. The locations of the suspicious lymph nodes were designated as parotid or mandibular. All lymph nodes on the right or left side were interpreted and the results were compared with the pathological findings.

The craniocaudal longitudinal diameters of the lymph nodes (maximum diameter) were measured on the selected T1-weighted and T2-weighted MR images. On the contrast-enhanced T1-weighted MR images, circular regions of interest (1.0−2.0 mm in diameter) were positioned on the hypointense area to determine signal intensities of the lymph nodes by consensus between the two radiologists. The signal intensity ratio was defined as the postcontrast signal intensity of an affected node relative to the adjacent muscle, and this was calculated for the metastatic and hyperplastic lymph nodes.

Histopathologic Analysis

After the MR images were obtained, the animals were sacrificed by administering a lethal dose (90 mg/kg) of intravenous sodium pentobarbital (Pentothal®, Choong Wae Pharmacy, Seoul, Korea). The parotid and mandibular lymph nodes were exposed to determine their positions and then they were carefully removed. The pathologic specimens were fixed in 10% phosphate-buffered formaldehyde for subsequent embedding in paraffin and the pathologic analysis. The histologic sections were obtained in planes paralleling the MR imaging orientations. Serial sections of the entire lymph nodes were obtained and subjected to hematoxylin-eosin (HE) staining, which was used to assess the lymph node morphology.

Two observers simultaneously reviewed all the slides with using a double-headed light microscope. The total number of nodes, the number of metastatic and hyperplastic lymph nodes, the number of necrotic metastatic nodes

and the maximum diameters of the nodes were documented. Discrepant interpretations were resolved by consensus.

Statistical Analysis

The mean sizes of metastatic and hyperplastic lymph nodes were compared by using the independent *t*-test in the SigmaStat 2.0 and SAS program for Windows version 11.0 (SPSS Science, Chicago, and the SAS Institute, Cary, NC). We investigated the use of node size and the signal intensity ratio as the criteria for the differentiation of metastatic and hyperplastic lymph nodes, and for calculating the accuracies, sensitivities, specificities and the positive and negative predictive values. Receiver operating characteristic (ROC) curve analyses were also performed by calculating the areas under the appropriate ROC curves (Az) (14). Binormal ROC curves were fitted using ROCKIT 0.9 software (15).

RESULTS

Histopathologic analyses of the 36 lymph nodes in six rabbits revealed 12 metastatic lymph nodes and 24 hyperplastic lymph nodes (Figs. 1, 2). For all the rabbits, lymphogenic metastasis was observed in the first draining parotid lymph node, except in one rabbit that showed lymphogenic metastasis in the caudal mandibular lymph node. Focal necrosis was identified in all the metastatic lymph nodes.

MR Imaging Findings

The size distributions of all the lymph nodes and the relations between the size measurements and the signal intensity ratios are shown in Figure 3. The average maximum diameters of the metastatic and hyperplastic lymph nodes were 10.5 $\pm$3.2 mm and 8.0 $\pm$3.6 mm, respectively, which was not statistically significant ($p >$

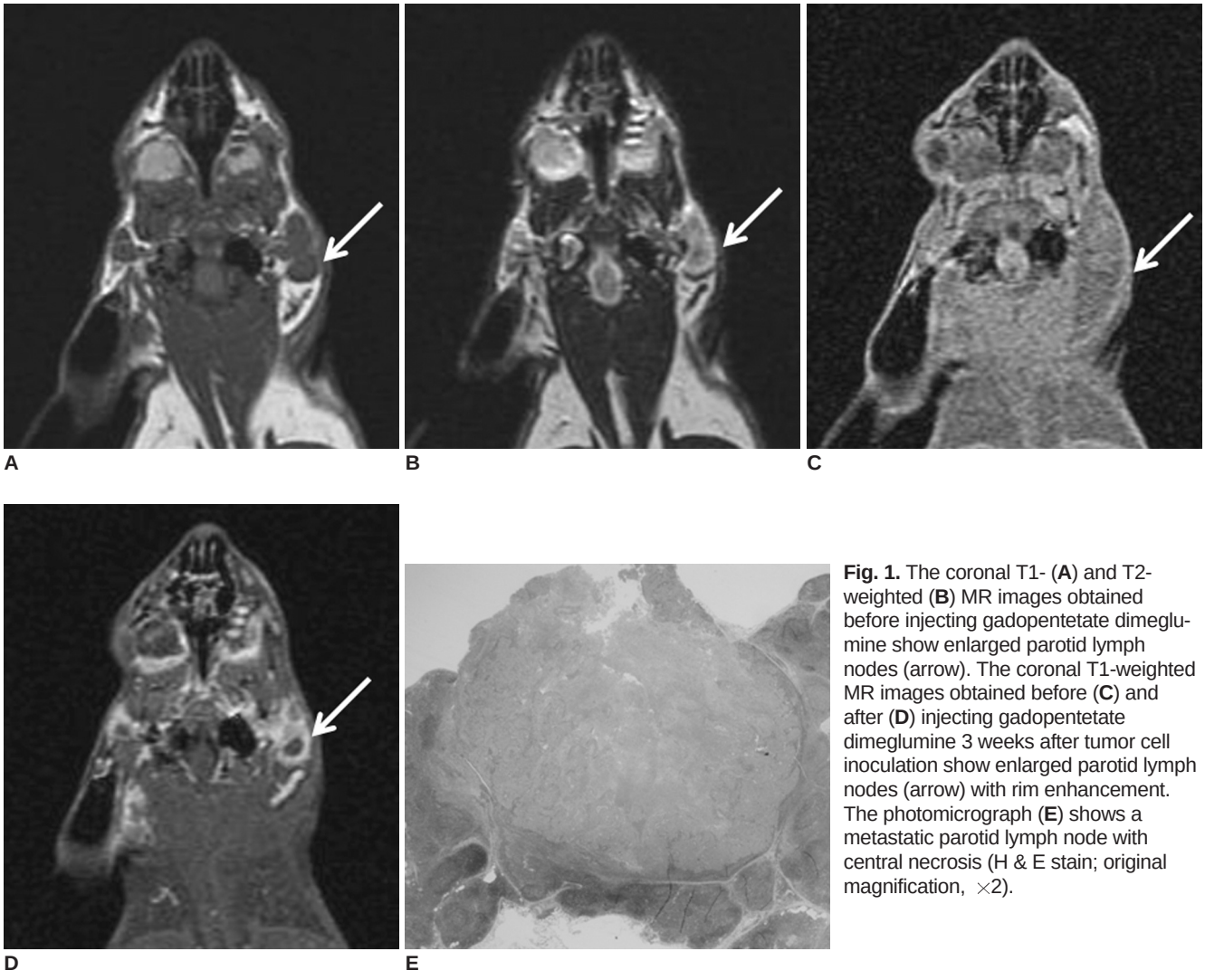

Fig. 1. The coronal T1- (**A**) and T2-weighted (**B**) MR images obtained before injecting gadopentetate dimeglumine show enlarged parotid lymph nodes (arrow). The coronal T1-weighted MR images obtained before (**C**) and after (**D**) injecting gadopentetate dimeglumine 3 weeks after tumor cell inoculation show enlarged parotid lymph nodes (arrow) with rim enhancement. The photomicrograph (**E**) shows a metastatic parotid lymph node with central necrosis (H & E stain; original magnification, $\times$2).

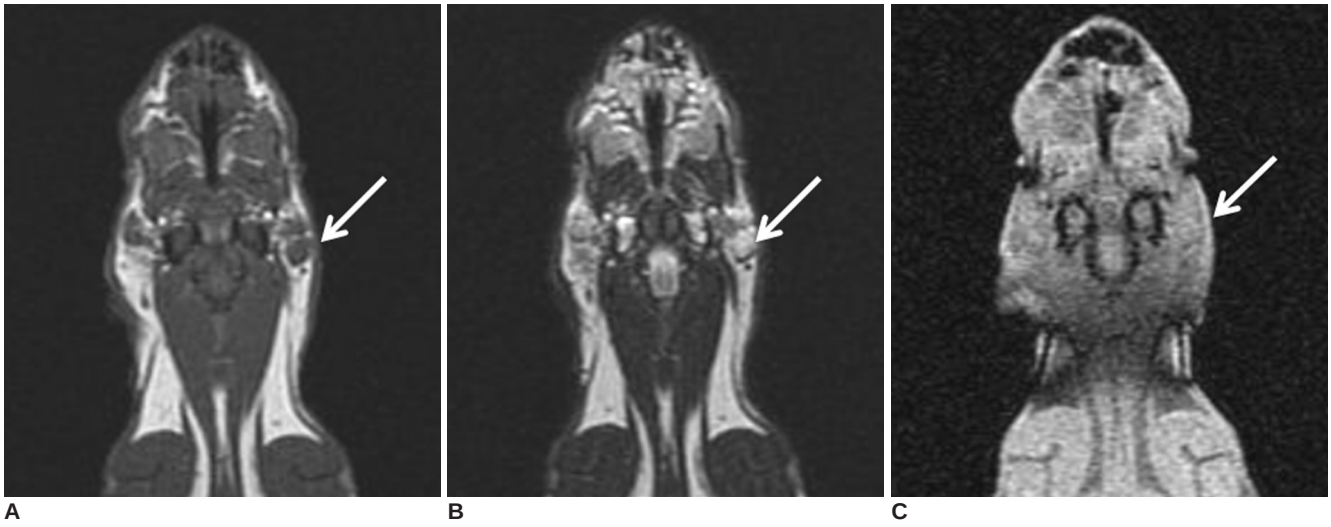

A B C

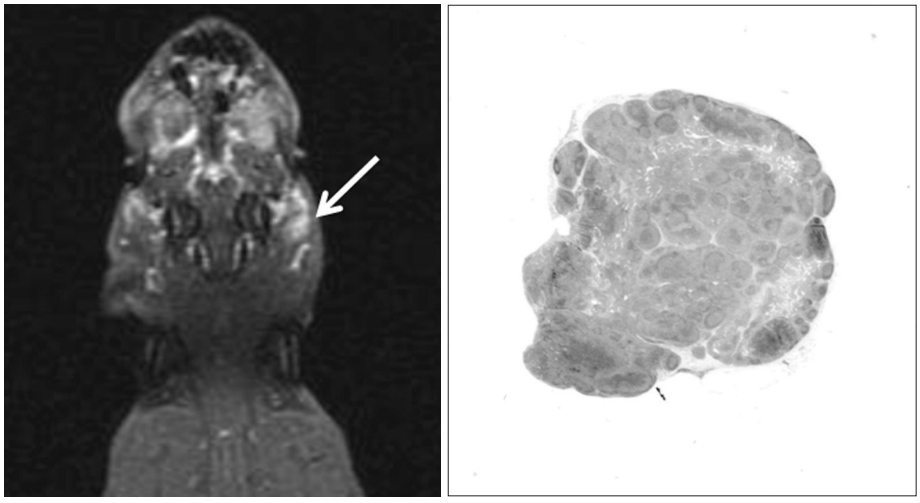

D E

Fig. 2. The coronal T1- (**A**) and T2-weighted (**B**) MR images obtained before injecting gadopentetate dimeglumine show enlarged parotid lymph nodes (arrow). The coronal T1-weighted MR images obtained before (**C**) and after (**D**) injecting gadopentetate dimeglumine at three weeks after tumor cell inoculation show enlarged parotid lymph nodes (arrow) with homogenous enhancement. The photomicrograph (**E**) shows a hyperplastic parotid lymph node (H & E stain; original magnification, ×2).

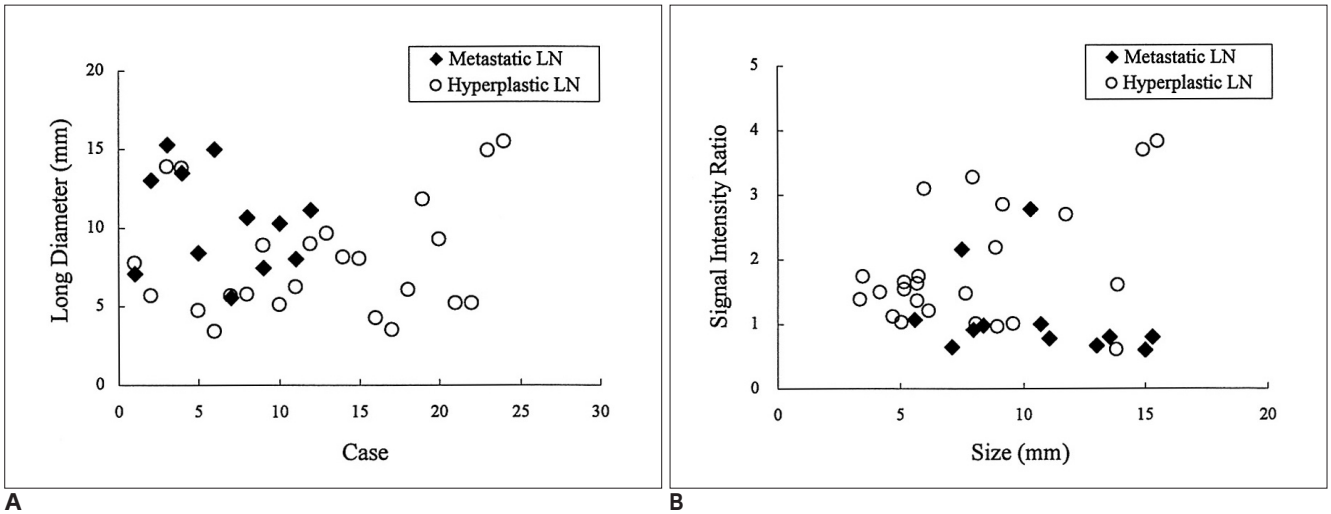

A B

Fig. 3. A. Graph showing the size distribution of the metastatic and hyperplastic lymph nodes in rabbits. The metastatic lymph nodes were larger (10.5±3.2 mm) than the hyperplastic nodes (8.0±3.6 mm), however, the difference was not statistically significant ($p > 0.05$).
B. Graph showing the signal intensity ratio of the metastatic and hyperplastic lymph nodes in rabbits with respect to the node size. The signal intensity ratio of the metastatic lymph nodes (0.82±0.16) was significantly lower than that of the hyperplastic lymph nodes (2.02±0.86) ($p < 0.05$). The size of the diseased lymph node and the signal intensity ratio was not found to be correlated ($p > 0.05$).

0.05). The mean signal intensity ratios of the metastatic and hyperplastic lymph nodes were 0.82 ±0.16 and 2.02 ± 0.86, respectively, which was statistically significant (p < 0.05). The correlation coefficient between the node size and signal intensity was 0.06, which was not statistically significant (p > 0.05)

The contrast-enhanced T1-weighted MR images showed peripheral high and central low signal intensity (n = 13) or homogenous high signal intensity (n = 23) (Figs. 1, 2). Of the 13 lymph nodes with peripheral high and central low signal intensity, nine nodes were confirmed to be metastatic (Fig. 1) and were four hyperplastic (Fig. 2) by microscopic examination. Of the 23 nodes with homogenous high signal intensity, three nodes were metastatic and 20 nodes were hyperplastic.

Diagnostic Accuracy

Using a cutoff value of a maximal diameter of 10 mm in the coronal plane, the sensitivity and specificity were 58% (7/12) and 79% (19/24), respectively, and they were 83% (10/12) and 50% (12/24), respectively, at a cutoff value of 7 mm. Using a signal intensity ratio less than one as a diagnostic criterion for a metastatic lymph node, the MR imaging had an accuracy of 81% (29/36), a sensitivity of 75% (9/12), a specificity of 83% (20/24), a positive predictive value of 69% (9/13) and a negative predictive value of 87% (20/23) for the detection of lymph node metastasis.

By ROC analysis, the Az value with a 95% confidence interval (CI) for a signal intensity ratio less than 1 on the contrast-enhanced T1-weighted MR images was 0.81 (95% CI: 0.63, 0.92), whereas that for a size measurement criterion of 10 mm was 0.72 (95% CI: 0.54, 0.86) (Fig. 4). The difference was significantly significant (p < 0.05).

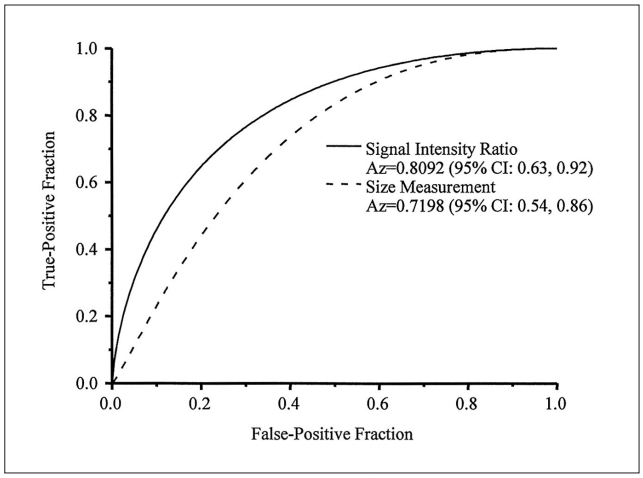

Fig. 4. Graph showing the receiver operating characteristic curves of size and signal intensity ratio for the detection of metastatic lymph nodes. The Az values were 0.81 for the signal intensity ratio and 0.72 for size as determined from the MR images, which were significantly different (p < 0.05). CI = confidence interval

DISCUSSION

The status of the cervical lymph nodes is one of the most important factors influencing the therapeutic management and outcome for patients suffering with head and neck squamous cell carcinoma. CT and MR imaging provide additional information regarding nodes that are inaccessible to palpation and the modalities may also show nodal necrosis, which is equated with tumor involvement in the appropriate clinical setting (16). These modalities can detect metastatic nodes in 38% to 67% of patients with no obvious nodal disease as revealed by clinical palpation (17). A tradeoff between sensitivity and specificity is necessary when only nodal size is considered. In our study, the sensitivity and specificity of MR imaging were 58% (7/12) and 79% (19/24), respectively, at a cutoff value of 10 mm, and they were 83% (10/12) and 50% (12/24), respectively, at a cutoff value of 7 mm.

Our experimental results show that the signal intensity ratios of lymph nodes according to MR imaging provide more useful information than the size criteria for the detection of regional metastatic lymph nodes in this head and neck carcinoma model. In our study, the 3D high-resolution MR images were obtained before and after injection of a conventional extracellular agent, i.e., gadopentetate dimeglumine. Nine (75%) of 12 metastatic cases showed peripheral high and central low signal intensity on the contrast-enhanced T1 weighted MR images. This enhancement pattern was histologically related to nodal necrosis. Dynamic contrast-enhanced MR imaging and the signal intensity curve analysis have recently been applied to the cervical lymph nodes in 21 patients with squamous cell carcinoma in the head and neck (18). A significantly longer time to peak, a lower peak enhancement, a lower maximum slope and a slower washout slope were found in tumor-involved lymph nodes compared with normal lymph nodes. The authors concluded that in the malignant lymph node there is a decreased transfer of contrast material to the tissue and a reduced volume of extracellular space (18).

New MR lymphotropic magnetic nanoparticles (19) and macrocyclic gadolinium chelates (8–10) have recently been shown to significantly improve the MR imaging diagnostic accuracy for nodal staging in animals and humans. Positron emission tomography (PET) using 18F-fluorodeoxyglucose (FDG) or integrated PET/CT is known to be a sensitive tool for the detection of hypermetabolic malignant lymph nodes (20). The described VX2 tumor

model in the rabbit could be used to compare the accuracies of using different imaging modalities or different contrast agents for nodal evaluations because as the present study shows, size criteria alone could not differentiate metastatic and hyperplastic regional lymph nodes in this model (21, 22). In the present study, tumor metastases to the parotid and/or mandibular lymph nodes developed in all the rabbits three weeks after auricular VX2 carcinoma inoculation. However, the limitations associated with the small number of animals examined during this study should be considered.

In conclusion, this experimental study confirms that metastatic and hyperplastic lymph nodes can be differentiated with using MR images and based on the contrast uptake patterns, but not based on any size criteria. This auricular VX2 carcinoma model could be used to compare the accuracies of the different imaging modalities or the different contrast agents for conducting lymph node evaluations.

References

1. Golder WA. Lymph node diagnosis in oncologic imaging: a dilemma still waiting to be solved. *Onkologie* 2004;27:194-199
2. O'Brien CJ, McNeil EB, McMahon JD, Pathak I, Lauer CS, Jackson MA. Significance of clinical stage, extent of surgery, and pathologic findings in metastatic cutaneous squamous carcinoma of the parotid gland. *Head Neck* 2002;24:417-422
3. Kau RJ, Alexiou C, Stimmer H, Arnold W. Diagnostic procedures for detection of lymph node metastases in cancer of the larynx. *J Otorhinolaryngol Relat Spec* 2000;62:199-203
4. Herborn CU, Vogt FM, Lauenstein TC, Goyen M, Dirsch O, Corot C, et al. Assessment of normal, inflammatory, and tumor-bearing lymph nodes with contrast-enhanced interstitial magnetic resonance lymphography: preliminary results in rabbits. *J Magn Reson Imaging* 2003;18:328-335
5. Kim SH, Kim SC, Choi BI, Han MC. Uterine cervical carcinoma: evaluation of pelvic lymph node metastasis with MR imaging. *Radiology* 1994;190:807-811
6. Moghimi SM, Bonnemain B. Subcutaneous and intravenous delivery of diagnostic agents to the lymphatic system: applications in lymphoscintigraphy and indirect lymphography. *Adv Drug Deliv Rev* 1999;37:295-312
7. Clement O, Luciani A. Imaging the lymphatic system: possibilities and clinical applications. *Eur Radiol* 2004;14:1498-1507
8. Misselwitz B, Platzek J, Weinmann HJ. Early MR lymphography with gadofluorine M in rabbits. *Radiology* 2004;231:682-688
9. Ruehm SG, Schroeder T, Debatin JF. Interstitial MR lymphography with gadoterate meglumine: initial experience in humans. *Radiology* 2001;220:816-821
10. Staatz G, Nolte-Ernsting CC, Adam GB, Grosskortenhaus S, Misselwitz B, Bucker A, et al. Interstitial T1-weighted MR lymphography: lipophilic perfluorinated gadolinium chelates in pigs. *Radiology* 2001;220:129-134
11. Dunne AA, Mandic R, Ramaswamy A, Plehn S, Schulz S, Lippert BM, et al. Lymphogenic metastatic spread of auricular VX2 carcinoma in New Zealand white rabbits. *Anticancer Res* 2002;22:3273-3279
12. Dunne AA, Plehn S, Schulz S, Levermann A, Ramaswamy A, Lippert BM, et al. Lymph node topography of the head and neck in New Zealand White rabbits. *Lab Anim* 2003;37:37-43
13. van Es RJ, Franssen O, Dullens HF, Bernsen MR, Bosman F, Hennink WE, et al. The VX2 carcinoma in the rabbit auricle as an experimental model for intra-arterial embolization of head and neck squamous cell carcinoma with dextran microspheres. *Lab Anim* 1999;33:175-184
14. Metz CE. Some practical issues of experimental design and data analysis in radiological ROC studies. *Invest Radiol* 1989;24:234-245
15. ROCKIT by Kurt Rossmann Laboratories, Department of Radiology, University of Chicago. Available at www-radiology.uchicago.edu/krl/KRL_ROC software _index.htm. Accessed June 10, 2005
16. Som PM. Detection of metastasis in cervical lymph nodes: CT and MR criteria and differential diagnosis. *AJR Am J Roentgenol* 1992;158:961-969
17. van den Brekel MW, Stel HV, Castelijns JA, Nauta JJ, van der Waal I, Valk J, et al. Cervical lymph node metastasis: assessment of radiologic criteria. *Radiology* 1990;177:379-384
18. Fischbein NJ, Noworolski SM, Henry RG, Kaplan MJ, Dillon WP, Nelson SJ. Assessment of metastatic cervical adenopathy using dynamic contrast-enhanced MR imaging. *AJNR Am J Neuroradiol* 2003;24:301-311
19. Anzai Y, Piccoli CW, Outwater EK, Stanford W, Bluemke DA, Nurenberg P, et al. Evaluation of neck and body metastases to nodes with ferumoxtran 10-enhanced MR imaging: phase III safety and efficacy study. *Radiology* 2003;228:777-788
20. Schoder H, Yeung HW, Gonen M, Kraus D, Larson SM. Head and neck cancer: clinical usefulness and accuracy of PET/CT image fusion. *Radiology* 2004;231:65-72
21. Choi SH, Moon WK, Hong JH, Son KR, Cho N, Kwon BJ, et al. Lymph node metastasis: ultrasmall superparamagnetic iron oxide-enhanced MR Imaging versus PET/CT in a rabbit model. *Radiology* 2007;242:137-143
22. Choi SH, Han MH, Moon WK, Son KR, Won JK, Kim JH, et al. Cervical lymph node metastases: MR imaging of gadoffluorine M and monocrystalline iron oxide nanoparticle 47 in a rabbit model of head and neck cancer. *Radiology* 2006;241:753-762